



## OPEN

## Interface-Induced Ordering of Gas Molecules Confined in a Small Space

## SUBJECT AREAS:

MOLECULAR SELF-  
ASSEMBLY

IMAGING TECHNIQUES

SURFACES, INTERFACES AND  
THIN FILMSYi-Hsien Lu<sup>1,2,3</sup>, Chih-Wen Yang<sup>1</sup>, Chung-Kai Fang<sup>1</sup>, Hsien-Chen Ko<sup>1</sup> & Ing-Shouh Hwang<sup>1</sup><sup>1</sup>Institute of Physics, Academia Sinica, Nankang, Taipei 115, Taiwan, R.O.C., <sup>2</sup>Nanoscience and Technology Program, Taiwan International Graduate Program, Institute of Physics, Academia Sinica, Taipei 115, Taiwan, R.O.C., <sup>3</sup>Department of Physics, National Taiwan University, Taipei 106, Taiwan, R.O.C.Received  
18 September 2014Accepted  
31 October 2014Published  
26 November 2014Correspondence and  
requests for materials  
should be addressed to  
I.-S.H. (ishwang@phys.  
sinica.edu.tw)

The thermodynamic properties of gases have been understood primarily through phase diagrams of bulk gases. However, observations of gases confined in a nanometer space have posed a challenge to the principles of classical thermodynamics. Here, we investigated interfacial structures comprising either O<sub>2</sub> or N<sub>2</sub> between water and a hydrophobic solid surface by using advanced atomic force microscopy techniques. Ordered epitaxial layers and cap-shaped nanostructures were observed. In addition, pancake-shaped disordered layers that had grown on top of the epitaxial base layers were observed in oxygen-supersaturated water. We propose that hydrophobic solid surfaces provide low-chemical-potential sites at which gas molecules dissolved in water can be adsorbed. The structures are further stabilized by interfacial water. Here we show that gas molecules can agglomerate into a condensed form when confined in a sufficiently small space under ambient conditions. The crystalline solid surface may even induce a solid-gas state when the gas-substrate interaction is significantly stronger than the gas-gas interaction. The ordering and thermodynamic properties of the confined gases are determined primarily according to interfacial interactions.

Gases exist throughout the universe and are essential in daily life as well as science and technology. Gases are generally defined as molecules that have boiling points below room temperature, such as the small nonpolar molecules N<sub>2</sub>, O<sub>2</sub>, He, and Xe. Gases are vapor under ambient conditions because van der Waals (VDW) interactions among gas molecules are much weaker than thermal energy. Condensing gas molecules into a liquid or solid state, based on the phase diagrams of bulk gases, requires high pressures or cryogenic techniques. However, numerous puzzling observations regarding gases confined in a small space have been reported. For example, gases have been observed to accumulate in a cap-shaped space on a nanometer scale at solid-water interfaces, mainly hydrophobic-water interfaces, under ambient conditions<sup>1–13</sup>. The cap-shaped structures are generally considered interfacial nanobubbles (INBs) that feature gas molecules in their vapor (gaseous) phase. However, their thermodynamic stability, nature, nucleation, and other properties and behaviors remain unclear. Theoretical prediction has indicated that gases inside a bubble of nanometer size should dissolve into the surrounding water in a short time<sup>14</sup> because of its high internal pressure,  $P_{in}$ , which can be described using the Young-Laplace equation,

$$\text{Laplace pressure } P_L = P_{in} - P_o = 2\Gamma/r \quad (1)$$

where  $P_o$  is the liquid pressure (approximately 1 atm in most laboratory conditions),  $\Gamma$  is the surface tension of the interface between liquid and gas, and  $r$  is the radius of the bubble (see Supplementary Note 1). Numerous atomic force microscopy (AFM) observations have shown that INBs are stable for hours or days<sup>1–12</sup>, which are at least 10–11 orders of magnitude longer than the theoretical lifetime estimated based on the Young-Laplace equation<sup>9</sup>. Another notable observation is quasi-two-dimensional (quasi-2D) micropancakes, which are layered structure of gas with a thickness of 0.3–10 nm and a width of sub-micron or micron size, on certain hydrophobic surfaces in air-supersaturated water<sup>15–18</sup>. These structures are as stable as INBs and occasionally INBs can be located on top of micropancakes. The nature of micropancakes remains unclear (see Supplementary Note 2).

Another example is the observation of liquid or solid nanoprecipitates of inert gases inside solids at room temperature<sup>19–35</sup>. These nanoprecipitates remain stable even at temperatures at which the precipitates can change shape and position or undergo coalescence. Compressive high pressures were expected for the condensation of inert gases. Generally, highly pressurized gases are thermodynamically unfavorable. Thus, it is unclear why these precipitates exhibit a high stability.



In this work, we conducted AFM studies of the interface between water and a hydrophobic substrate, highly ordered pyrolytic graphite (HOPG), in water supersaturated with either oxygen or nitrogen. These two gases were chosen because they are the two major components of air. Both gases exhibited ordered epitaxial base layers and cap-shaped soft nanostructures resembling INBs. The latter were probably liquid-like gas agglomerates at the HOPG-water interface. Regarding oxygen, structures resembling the micropancakes were observed and they exhibited disordered dense gas layers on top of the ordered base layers. We conclude that the ordering of nitrogen and oxygen inside these interfacial structures is induced by the crystalline HOPG substrate and further stabilized by the interfacial water on the top. These interfacial structures comprising gas molecules may possess novel properties that can explain several scientific problems. Understanding the underlying mechanisms may enable numerous technological applications. In addition, the interface-induced ordering can be generalized to understand previous observation of the solid or liquid nanoprecipitates of inert gases inside solids and other phenomena.

## Results

### AFM study of the structures of oxygen at the HOPG-water interface.

After oxygen-supersaturated water was deposited onto a clean

HOPG sample, we observed considerably complex interfacial structures. A typical case is shown in Figs. 1, 2, and supplementary Figs. S1–S4. We used two advanced AFM techniques, the frequency-modulation (FM) and PeakForce (PF) modes, because each has distinct advantages in probing the interfacial structures. Here,  $t$  is defined as 0 when the water is deposited onto the HOPG surface. Only the late stage of growth is shown because the interface was highly dynamic following water deposition.

Figure 1 shows FM-AFM images of the interfacial structures. Cap-shaped nanostructures were present and tended to be located on top of thick pancake-shaped layers (Figs. 1a and 1b). The thicknesses of the quasi-2D structures varied among areas (Fig. 1a). High-resolution imaging indicated no bare HOPG region (Figs. 1b and 1c). The lower (darker) regions were the ordered base layers, which featured thicknesses varying from one to four monolayers and comprised domains of two sets of row-like patterns. The ordered structures can be discerned easily in the dissipation image (Fig. 1d). Bright (high dissipation) regions exhibited row-like patterns with row separation of 4–5 nm, and dark (low dissipation) regions are featureless, suggesting that the pancake- and cap-shaped structures were disordered. In Fig. 1c, a few small disordered regions were only approximately 0.5 nm higher than the neighboring ordered structure, suggesting that one disordered molecular layer was located on top of the ordered

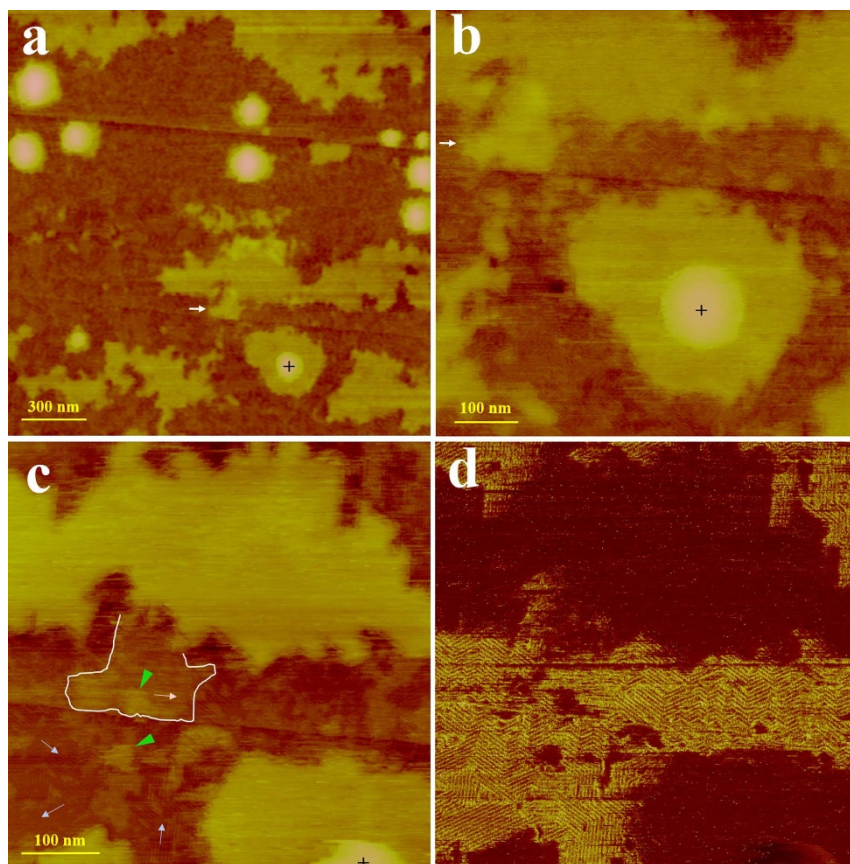


**Figure 1** | FM-AFM measurements of a HOPG-water interface after oxygen-supersaturated water was deposited. (a) Topographic image acquired at  $t = 300$  min. A cap-shaped nanostructure marked with “+” serves as a marker for comparison with other images. (b) Higher-resolution height image of a region around the cap-shaped nanostructure marked with “+” acquired at  $t = 310$  min. Because of the large height variation of various structures, the contrast of the row-like patterns in the base layers cannot be clearly shown. (c) Topographic image of a similar area acquired at  $t = 205$  min. The region outlined by white lines was later covered by a thick disordered layer, as indicated by the white arrow in (a) and (b). In the ordered base layers, two sets of row-like structures existed; one set was oriented along a zigzag direction (indicated using pink arrows) of the HOPG substrate and the second was oriented along an arm-chair direction (indicated using blue arrows). The green arrow indicates areas with a disordered molecular layer. (d) Dissipation image acquired simultaneously with the image shown in (c). We note that primarily flat terraces and substrate step edges were observed when pre-degassed water was deposited on clean HOPG<sup>36–38</sup>. Domains of monolayer row-like patterns might appear, but the coverage was typically less than 10% of the interface after 8 hours of water deposition. Thus the 2D and 3D patterns shown here were produced by oxygen accumulating at the interface.

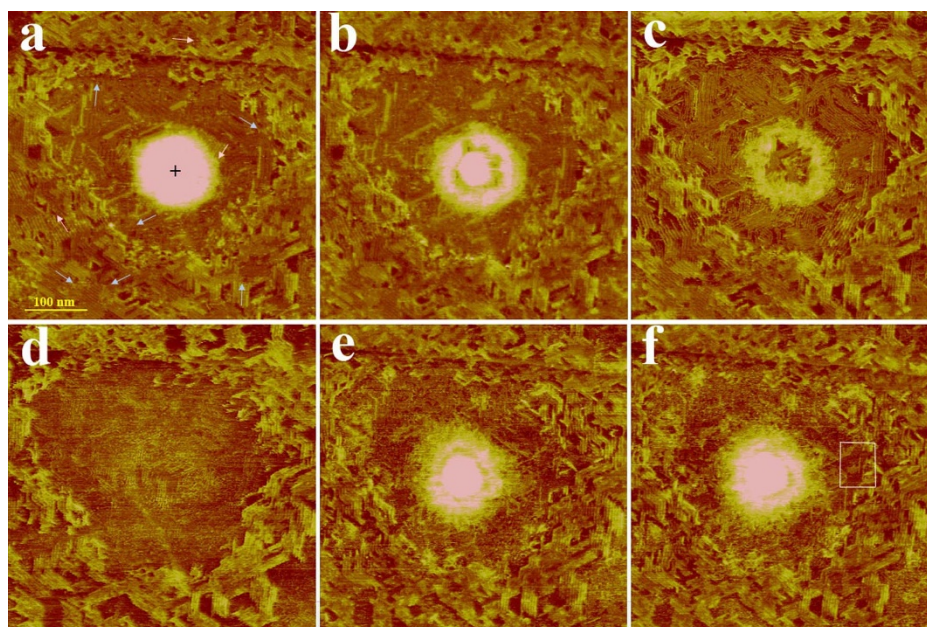


**Figure 2 | Height images of a HOPG-water interface acquired with PF mode after oxygen-supersaturated water was deposited.** Peak forces of +100 pN (a), +250 pN (b), +650 pN (c), +1250 pN (d) were applied. The peak force was returned to 100 pN in (e) and (f). In the region corresponding to the thick pancake-shaped layer, the tip penetrated through the disordered layer to image the underlying ordered base layers, which appeared approximately 0.5 nm lower than the surrounding ordered layers. Ordered structures, comprising two sets of three rotated row-like structures, were observed. One set with the rows oriented along the arm-chair directions is indicated using blue arrows and the second set, which was oriented along the zig-zag directions, is indicated with pink arrows. The outlined region in (f) indicates an area showing formation of new ordered structures.

base layers. Most thick pancake-shaped layers were 2–4 nm higher than the base layers (Supplementary Fig. S1), and their shape and thickness resembled those of the micropancakes reported in previous AFM studies<sup>15–18</sup>. Our extensive investigation of the HOPG–water interface under various conditions indicated that the thick pancake-shaped structures appear only when water is supersaturated with air or oxygen. These structures have never been observed when pre-degassed water<sup>36–38</sup> or water saturated<sup>39</sup> or supersaturated with pure nitrogen is used (please refer to Fig. 3). This strongly suggests that micropancakes form through the precipitation of oxygen molecules at the interface.

When we switched to the PF mode to study the interface, domains of row-like patterns were observed in regions originally exhibiting thick disordered pancake-shaped structures. An example is shown in Fig. 2a and Supplementary Figs. S2 and S3. These patterns were similar to the surrounding ordered base layers, although their heights were approximately one molecular layer lower. The cap-shaped nanostructures could still be seen, but their apparent heights were significantly smaller than those measured with the FM mode (Supplementary Figs. S1–S3). Our measurements of force versus tip-sample separation, or force curves, indicate a snap-in when the tip touched a cap-shaped nanostructure or a thick pancake-shaped layer (Supplementary Fig. S4). The tip penetrated into the structures to a certain depth, rather than traced their interfaces with water, to offset the attractive snap-in force. For the same reason, the tip revealed domains of the stiff ordered structures under the pancake-shaped disordered layer. Growth of a thick disordered layer on top of the ordered base layers was observed in the region outlined by white lines in Fig. 1c compared with subsequently acquired images shown in Figs. 1a and 1b. We probed several areas on this sample and observed ordered base layers beneath all disordered quasi-2D structures. Similar structures were also observed for micropancakes at the HOPG-water interface when the water was supersaturated with air.

The apparent height of the cap-shaped nanostructure decreased as the peak force increased (Figs. 2 a–d) because the tip penetrated deeper into the structure. When the peak force was increased to

+650 pN, ordered row-like structures under the cap-shaped nanostructure became visible (Fig. 2c). When the peak force was increased to +1250 pN (Fig. 2d), the cap-shaped nanostructure was not observed and numerous regions of the ordered structures were seemingly destroyed by the high force and became fuzzy, particularly the region under the thick pancake-shaped layer. When the peak force was returned to +100 pN (Fig. 2e), the cap-shaped nanostructure appeared again, but its apparent width and height substantially decreased compared with those shown in Fig. 2a. In addition, the structures in numerous areas of the base layers remained fuzzy, indicating disordering in those areas after imaging with the high peak force. After continuous imaging using a low peak force (Fig. 2f), ordered row-like structures gradually appear in the fuzzy regions over the time scale of minutes or longer.

As shown in Supplementary Figs. S2b–S2d, the thick pancake-shaped layers and cap-shaped nanostructures exhibited similar mechanical contrasts in the corresponding adhesion, stiffness (DMT modulus), and deformation maps, which were considerably different from those of the ordered base layers. Several mechanical properties of INBs and micropancakes at the HOPG-water interface prepared using the standard solvent exchange method<sup>2</sup> were also measured with the PF mode. The similar shapes, dimensions, and mechanical properties indicated that the cap-shaped nanostructures (thick pancake-shaped layers) were probably the INBs (micropancakes).

#### AFM study of the structures of nitrogen at the HOPG-water interface.

When nitrogen-supersaturated water was deposited onto a clean HOPG sample, cap-shaped nanostructures and patches of monolayer ordered structures were observed at the HOPG-water interface. A typical example is shown in Supplementary Fig. S5. A more detailed characterization of the interfacial structures using the PF mode is shown in Fig. 3. The ordered structure was oriented along one of three equivalent zig-zag directions of the HOPG substrate, the lattice of which was imaged using the contact mode (Supplementary Fig. S6). The structure exhibited the same

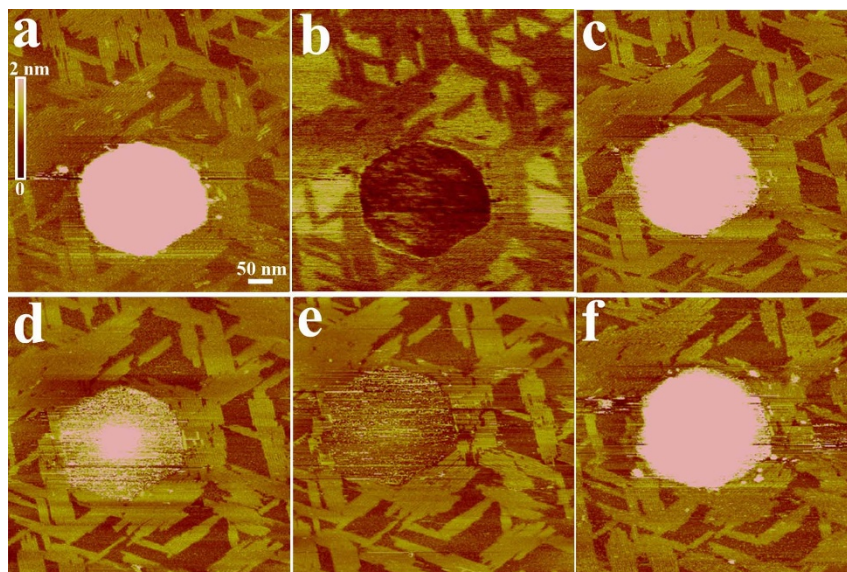


**Figure 3 | Images of an HOPG-water interface acquired using the PF mode at approximately 4 hours after nitrogen-supersaturated water was deposited.** (a), (c), (d), (e), and (f) are height images. The peak force used to acquire (a) and (b) was 150 pN. Peak forces of 750 pN (c), 1500 pN (d), and 2250 pN (e) were applied and, finally, the force was reduced to 150 pN (f). The apparent heights at the center of the cap-shaped structure in (a), (c), (d), (e) and (f) were 18.5 nm, 10.2 nm, 2.7 nm, 0.2–0.4 nm, and 12.6 nm, respectively. The left edge of the 3D nanostructure in (f) exhibited several changes after applying a peak force of 2250 pN. The real height of the cap-shaped nanostructure after the PF measurements was 20.3 nm, which was determined from the force curve measurements conducted at the center of the structure (see Supplementary Fig. S7). The domains of the row-like structure changed slowly with time. Furthermore, several domains exhibited damage at high peak forces (e.g., domains near the left edge of the cap-shaped structure). (b) is the corresponding adhesion map acquired along with (a). Both the cap-shaped nanostructure and the monolayer ordered structure appeared darker than the bare HOPG substrate. In (f), an increasing number of bright particles with heights ranging from 0.8 nm to 3 nm appeared after scanning with a high peak force.

appearance as that reported at the HOPG-water interface using pre-degassed water in a nitrogen or air environment<sup>36–39</sup>. Figure 3a is a height image acquired at a peak force of 150 pN. No specific pattern was observed inside the cap-shaped structure in the corresponding adhesion map (Fig. 3b), suggesting a disordered structure.

As shown in Figs. 3a–3e, the apparent height of the cap-shaped nanostructure decreased as the peak force was increased. When the peak force reached 2250 pN, the apparent height decreased to nearly zero (Fig. 3e) and no underlying structure was observed, indicating that the bare HOPG substrate was under the cap-shaped nanostructure. The cap-shaped nanostructure was surrounded by domains of the row-like pattern, forming the hexagonal boundaries of the structure. When the peak force was reduced from 2250 pN to 150 pN, the cap-shaped structure reappeared (Fig. 3f). However, the apparent height decreased from the 18.5 nm shown in Fig. 3a to 12.6 nm. This probably occurred because scanning at the maximal peak force of 2250 pN strongly perturbed the structure, causing dissolution or removal of gas molecules inside the cap-shaped nanostructure. The increasing number of small bright particles that appeared on the surrounding row-like structure in Fig. 3f might have been engendered by the gas inside the cap-shaped nanostructure and the destruction of areas of the monolayer ordered structure. These particles frequently changed sites and disappeared after one to several scans. This observation is similar to our recent FM-AFM observations at the HOPG-water interface in a nitrogen environment<sup>39</sup>.

**Schematics of interfacial structures and the role of interfacial water.** Based on the aforementioned observations and many similar experiments conducted at the HOPG-water interface, schematics for the interfacial structures of nitrogen and oxygen are illustrated in Fig. 4 (For more detailed description, please see Supplementary Note 3). This work showed that the thick pancake-shaped layers are primarily dense disordered layers of oxygen adsorbates on top of the ordered base layers of oxygen. This

discovery explains a previous report that micropancakes form on crystalline hydrophobic substrates<sup>18</sup>, because the epitaxial base layers can form only on crystalline substrates. We speculate that the structures in quasi-2D disordered layers have a certain degree of short-range order in the lateral directions that is attributable to interaction with the underlying ordered base layers; however, structural fluctuations occur faster than our AFM imaging rate ( $\sim 1$  ms per pixel or  $\sim 0.5$  s per line). Researchers have recently suggested that micropancakes are 2D dense gas adsorbates<sup>9,10</sup>. Our observations provide evidence supporting this suggestion, but the underlying ordered base layers were not expected.

Through strong perturbation using the AFM tip, a micropancake can be transformed into an INB with no significant change in the total volume<sup>17</sup>, indicating that the material density of the two structures is similar. This finding is consistent with those of the current study, which revealed that the various mechanical properties of these two structures measured using the PF mode and force curves are similar. Thus, the cap-shaped nanostructures are probably 3D disordered structures containing close-packed gas molecules. They can be considered 3D liquid-like nanodroplets comprising gases rather than bubbles in the low-density vapor phase<sup>40</sup> (see Supplementary Note 4).

The observation of INBs on micropancakes indicates that the chemical potentials of gas molecules inside the two structures are similar<sup>16</sup>. INBs can be moved by using an AFM tip on the top plateau of a micropancake<sup>15</sup> and two INBs on the same micropancake may coalesce into a larger INB<sup>16</sup>. A thin water layer was suggested to separate these two structures<sup>15</sup>. The current study revealed no notable gas transfer among the cap-shaped nanostructures, the pancake-shaped layers, and the ordered adlayers, as well as between these interfacial structures and the surrounding water over a timespan of several minutes. Interfacial water layers probably stabilized the interfacial structures of gases by reducing the interfacial energy. They also act as a barrier to hinder gas transfer among the interfacial structures

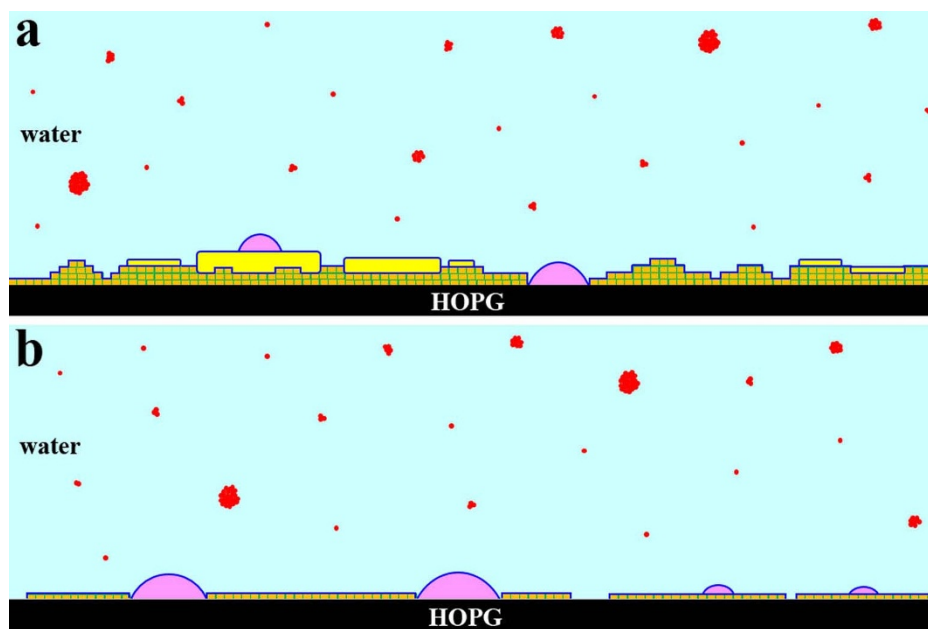


**Figure 4** | Schematic of the structures at the HOPG-water interface when water is supersaturated with pure oxygen (a) and pure nitrogen (b). For clarity, some structures may not be represented in the correct scale. Orange squares represent ordered structures; cap-shaped nanostructures and small nitrogen and oxygen clusters at the interface are shown in purple; 2D disordered layers are shown in yellow; and gas molecules dissolved in water are shown in red. Each red sphere represents an individual gas molecule and some molecules can aggregate into clusters in water. The interfacial water layers that stabilize these 2D and 3D nitrogen and oxygen structures are shown in deep blue.

and between the structures and surrounding bulk water (see Supplementary Note 5). This explains several experimental observations presented in this paper and other AFM studies. The interfacial water layers may have special structural configurations, which require further experimental and theoretical investigations.

**Thermodynamic stability of the interfacial structures of gas molecules.** A recent TEM study reported that hydrogen INBs can be generated in an aqueous solution by using electron radiolysis<sup>13</sup>. The INBs were estimated to have a high gas density at room temperature. If INBs are in a “dense gas” phase, high pressure is expected, and induces strong water flow from INBs. However, tracer particle tracking measurements indicated no water flow around the INBs<sup>11</sup>. In addition, INBs have a planar interface with micropancakes and thus no pressure drop occurs between INBs and micropancakes. Micropancakes are 2D interfacial structures of which the internal pressure should be equal to the pressure in the surrounding water, approximately 1 atm. We thus conclude that the pressure inside INBs is not much higher than 1 atm.

Numerous experiments suggest that INBs at hydrophobic-water interfaces are probably thermodynamically stable under ambient conditions. For example, INBs can be formed in water with air near saturation level<sup>10</sup> and most INBs are stable for hours or days<sup>1–12</sup>. These facts indicate that the chemical potentials of gases in INBs are equal to or lower than those in ambient air. This precludes the possibility that INBs are hyperbaric gaseous bubbles because gases inside pressurized bubbles have higher chemical potentials than gases in ambient air do (see Supplementary Note 6).

Our previous AFM observations have indicated that dissolved nitrogen molecules can be adsorbed at the HOPG-water interface and form a monolayer row-like structure even in under-saturated water<sup>36–39</sup>, suggesting that HOPG, a hydrophobic solid substrate, in water may provide sites of low chemical potential at which dissolved gas molecules can be adsorbed. This is probably because the attractive VDW interactions between gas molecules and the hydrophobic substrate, as well as the interactions between adsorbed gas structures and the interfacial water, are responsible for reducing the chemical

potentials. This mechanism also explains the formation and high stability of the various interfacial structures of gases at the hydrophobic-water interfaces.

**Relevance to the nanoprecipitates of inert gases in solids.** Inert gas atoms exhibit low solubility in most solids and form nanoprecipitate when implanted into solids; this behavior is analogous to the behavior of nonpolar gas molecules in water. The most unexpected discovery was the extremely high atomic densities (equivalent to those in solid or liquid states) of inert gas atoms within the small cavities of the host solids at room temperature<sup>19–35</sup>. In particular, solid phase precipitation of the heavy inert gases (Ar, Xe, Kr) in metals<sup>24–33</sup> and crystalline Si have been reported<sup>35</sup>. The solid nanoprecipitates exhibited a structure epitaxial with the host matrix. The most commonly studied system is that of Xe in Al thin films of approximately 50 nm. Xe can be condensed into a close-packed solid state when confined in Al cavities with diameters smaller than 6 nm and into a liquid state when confined in a cavity larger than 10 nm<sup>30–32</sup>. High pressure (several to hundreds of thousands of atmospheres) was expected in the nanoprecipitates based on the phase diagrams of bulk gases. The Young-Laplace equation was applied to explain the solid and liquid phases of precipitates of different sizes, because a higher Laplace pressure is expected inside a smaller spherical cavity. However, there are observations indicating that this equation cannot provide adequate estimation of the pressure inside these nanoprecipitates (see Supplementary Note 7).

This study showed that ordered epitaxial adlayers of oxygen and nitrogen, solid-gas phases, can form at an HOPG-water interface under ambient conditions. HOPG is atomically flat and, thus, no high pressure is expected inside the ordered gas adlayers. This proves that compressive high pressure is not essential for the formation of the solid-gas phase. A TEM study reported that semicrystalline Xe precipitates exhibited a solid phase in the first three layers adjacent to the crystalline Al substrate and a liquid phase in their center<sup>32</sup>. This implies that the solid structure of Xe atoms is induced by the crystalline substrate; this process is analogous to the formation of the first



Table 1 | Gas-solid and gas-gas interactions

Gas-solid	Potential Well Depth (meV) <sup>a</sup>	Gas-Gas	6–12 Lennard Jones Potential Well Depth (meV) <sup>b</sup>	Dispersion Interaction (meV) <sup>c</sup>
N <sub>2</sub> -Graphite	104 ± 3	N <sub>2</sub> -N <sub>2</sub>	7.89	9.1
O <sub>2</sub> -Graphite	90.4~101.7	O <sub>2</sub> -O <sub>2</sub>	9.75	10.5
Ar-Graphite	96 ± 2	Ar-Ar	10.70	11.1
Ar-Ag(111)	72 ± 7			
Xe-Graphite	162 ± 4	Xe-Xe	19.75	21.5
Xe-Cu(111)	172~194			
Xe-Pd(111)	356			
Xe-Pt(111)	269~304			
Xe-W(110)	180 ± 6			
Xe-Al(111)	176			
He-Graphite	16.2~17.0	He-He	0.88	
He-Ag(111)	6~7			
He-Cu(110)	6.27 ± 0.8			
He-W(110)	3.5			
He-Pt(110)	8.5 ± 0.2			

<sup>a</sup>The values of the potential well depth are mainly taken from Ref. 44, but the value for Xe-Al is taken from Ref. 45.

<sup>b</sup>The values of Lennard Jones Potential Well Depth are taken from Ref. 42.

<sup>c</sup>The values of dispersion interaction are calculated as described in methods.

one to four ordered adlayers of nitrogen and oxygen at the HOPG-water interface. Strong interactions between gas and a solid surface relative to the gas-gas interactions are a key factor in the ordering of gas in our system as well as in inert-gas precipitates inside solids.

The VDW interaction energy between gas molecules can be estimated based on the latent heat of sublimation<sup>41</sup> or the viscosity coefficient<sup>42</sup>. Gas-solid interactions have been a key research topic in surface science for decades<sup>43–45</sup>. One rarely-known fact is that gas-solid interactions are often considerably stronger than gas-gas interactions (by one order of magnitude), as shown in Table 1. For example, the energy values of N<sub>2</sub>-N<sub>2</sub>, N<sub>2</sub>-HOPG, O<sub>2</sub>-O<sub>2</sub>, O<sub>2</sub>-HOPG, Xe-Xe, and Xe-metal interactions are approximately 9 meV, 100 meV, 10 meV, 100 meV, 22 meV, and 200–400 meV, respectively. The strong interfacial interaction between gas molecules and solid substrates is conducive to condensation of the gases confined in solids or at a solid-liquid interface. In addition, the crystalline substrate provides a periodic corrugation of holding potentials for the adsorbates, which may drive the solid ordering of the gas molecules. This interface-induced ordering weakens when the molecules are located farther from the interface. Thus, the ordered adlayers persist for only a few atomic or molecular layers, explaining our observation of the first one to four ordered adlayers at the HOPG-water interface and previous observations of the solid-gas precipitates inside the small cavities of the solids (see Supplementary Note 8).

## Discussion

Hwang et al. proposed that the formation of a gas agglomerate (a gas cluster) in water or at a solid-water interface is energetically favorable to the formation of a gaseous bubble when the number of confined gas molecules,  $N$ , is lower than a critical size  $N_c$ <sup>36,38</sup>. This concept can be understood qualitatively. For a small structure, the ratio of interfacial (surface) area to volume increases as the size decreases, and the contribution of the interfacial (surface) energy to the total free energy becomes more dominant. Therefore, the thermodynamic properties of gas molecules confined in a medium (such as a solid, water, a solid-water interface, or other materials in a condensed state) of a sufficiently small space can be considerably different from those of bulk gases. Interfacial energy is generally positive and roughly proportional to the interfacial area, which favors a condensed state rather than a gaseous state<sup>36,38</sup>. In addition, the energy per unit area for cluster-water (cluster-solid) interfaces should be substantially lower than that for vapor-water (vapor-solid) interfaces because of the additional attractive VDW interactions for the former interfaces.

The critical size,  $N_c$ , increases as the interfacial interaction between gas molecules and the medium becomes stronger. This concept can be generalized to a precipitate or a material embedded inside another material or located at interfaces of other materials. This indicates that the thermodynamic properties of an inclusion may be dominated by the interaction energy at the interface when its size is sufficiently small.

INBs are 3D liquid-like gas structures, which may have distinct physical properties. The mutual interactions among gas molecules are merely weak VDW forces, and thus INBs may shear easily and behave as a low-viscosity liquid. This can reduce the friction for motion of a solid above INBs and drag for water flow above. The presence of a low-viscosity layer at the solid-water interface was suggested to explain the boundary slip and drag reduction of water flow<sup>46</sup>, but the physical origin of the low-viscosity layer remains unclear. The VDW liquid in INBs may provide a clue that can be used in determining the mechanism. The findings and explanations presented in this paper may clarify numerous puzzles regarding gases confined in a small space and have implications regarding various research fields. For example, hydrophobic surfaces can effectively catch gases dissolved in water; this property may have implication regarding the breathing of marine species and other phenomena. In addition, gases dissolved in aqueous solutions may affect the self-assembly and functions of biological molecules. Furthermore, interface-induced ordering provides new possibilities for high-density gas storage.

## Methods

**Sample preparation.** The highly ordered pyrolytic graphite (HOPG) samples (lateral sizes of 12 mm × 12 mm, ZYB; Momentive) were freshly cleaved with scotch tape prior to each AFM experiment. All water was purified using a Milli-Q system (Millipore Corp., Boston) with a resistivity of 18.2 MΩ·cm. In preparation of water supersaturated with nitrogen (oxygen), a beaker containing DI water (30–50 mm high) was placed in a pressure tank (TNKB1-3; Misumi) which was pumped to ~0.05 atm for several min with an oil-free vacuum pump (Rocker 410, Rocker) and then pressurized to 2.4–3.7 atm with high-purity (99.999%) nitrogen (oxygen). An air filter (MSAF8A-0.01, Misumi) with a filtration level of 0.01 μm was used between the high pressure gas cylinder and the stainless-steel pressure tank. The water was stored for several days. Right before the AFM experiments, the chamber was opened and the water was extracted and injected to the AFM liquid cell using a disposable syringe (5 ml) with a silicone tube. All of the experiments were conducted at room temperature.

**Atomic force microscopy.** The images in this paper were acquired using a Bruker AXS Multimode NanoScope V equipped with a commercial fluid cell tip holder. A schematic of the setup is shown in Supplementary Fig. S8a. The oscillation of the cantilever was driven using a dynamic-modulation system composed of a lock-in unit/phase-lock-loop (PLL) unit (Nanonis OC4 Station from SPECS) and a signal access module (Bruker AXS). For the frequency-modulation (FM) mode, the PLL unit



was employed to track the resonance frequency of the vibrating cantilever. The resonance frequency shift ( $\Delta f$ ) was used as the feedback input signal of a proportional-integral controller to obtain topographic images. The driving amplitude, which was controlled using the PLL to maintain a constant cantilever oscillation amplitude during scanning, could be measured and recorded simultaneously. This value was typically considered the energy dissipation signal<sup>47</sup>. A dissipation map was obtained along with the topographic images. The FM detection scheme was used here because it has exhibited superior force sensitivity compared with the conventional tapping mode<sup>36–38,48–50</sup>. The sample displacement was driven using a piezoscanner under the sample stage. Si cantilevers (OMCL-AC240TS from Olympus) with a spring constant 0.7–3.8 N/m were used. The nominal tip radius was approximately 10 nm. The resonance frequency of the cantilever was approximately 32 kHz in water. For operation using the FM mode, the resonance amplitude was 3.6 nm and the resonance frequency shift was set at +10 to +15 Hz.

**PeakForce (PF) mode.** Regarding the PeakForce mode, the sample was oscillated in a vertical direction with an amplitude of tens to hundreds of nanometers and at a frequency of 2 kHz (Supplementary Fig. S8b). The vertical piezo movement results in cycles of approaching and retracting traces in which the tip makes intermittent contact with the sample surface. A force-distance curve was acquired in each cycle. Topography information was obtained from the height correction performed by the feedback loop to keep a constant “peak” of force, whereas the slope of the force curve at the contact region determined the stiffness of the sample at each pixel. Other information on the surface mechanics, such as adhesion, deformation, or dissipation, was obtained using the measured cycle of the approach-retraction force curve, as shown in Supplementary Fig. S8b<sup>51,52</sup>. In the operation, the scan rate was approximately 1 Hz and the oscillation amplitude was 15–25 nm.

**Calculation of the Dispersion Interaction.** The molar cohesive energy ( $U$ ) for a van der Waals solid can be estimated with the latent heat of melting ( $L_m$ ) plus vaporization ( $L_v$ )<sup>41</sup>.  $L_m$  for N<sub>2</sub>, O<sub>2</sub>, Ar, and Xe are 0.71, 0.44, 1.18 and 2.27 kJ/mol (at the melting point, 1 atm), respectively;  $L_v$  for N<sub>2</sub>, O<sub>2</sub>, Ar, and Xe are 5.57, 6.82, 6.43 and 12.57 kJ/mol (at the boiling point, 1 atm), respectively<sup>53</sup>. Assuming these molecules form closely packed structures with 12 nearest neighbors per atom at low temperatures, the strength of dispersion interaction ( $C_{disp}$ ) can be calculated as<sup>41</sup>

$$U = L_m + L_v = 7.22N_0 C_{disp} \quad (2)$$

where  $N_0$  denotes the Avogadro constant.

- Ishida, N., Inoue, T., Miyahara, M. & Higashitani, K. Nano bubbles on a hydrophobic surface in water observed by tapping-mode atomic force microscopy. *Langmuir* **16**, 6377–6380 (2000).
- Lou, S. T. *et al.* Nanobubbles on solid surface imaged by atomic force microscopy. *J. Vac. Sci. Technol. B* **18**, 2573–2575 (2000).
- Tyrrell, J. W. G. & Attard, P. Images of nanobubbles on hydrophobic surfaces and their interactions. *Phys. Rev. Lett.* **87**, 176104 (2001).
- Zhang, X. H., Li, G., Maeda, N. & Hu, J. Removal of induced nanobubbles from water/graphite interfaces by partial degassing. *Langmuir* **22**, 9238–9243 (2006).
- Zhang, L. J. *et al.* Electrochemically controlled formation and growth of hydrogen nanobubbles. *Langmuir* **22**, 8109–8113 (2006).
- Zhang, X. H., Khan, A. & Ducker, W. A. A nanoscale gas state. *Phys. Rev. Lett.* **98**, 136101 (2007).
- Zhang, X. H., Quinn, A. & Ducker, W. A. Nanobubbles at the interface between water and a hydrophobic solid. *Langmuir* **24**, 4756–4764 (2008).
- Craig, V. S. J. Very small bubbles at surfaces—the nanobubble puzzle. *Soft Matter* **7**, 40–48 (2011).
- Seddon, J. R. T. & Lohse, D. Nanobubbles and micropancakes: gaseous domains on immersed substrates. *J. Phys.: Condens. Matter* **23**, 133001 (2011).
- Seddon, J. R. T., Kooij, E. S., Poelsema, B., Zandvliet, H. J. W. & Lohse, D. Surface bubble nucleation stability. *Phys. Rev. Lett.* **106**, 056101 (2011).
- Chan, C. U. & Ohl, C. D. Total-Internal-Reflection-Fluorescence Microscopy for the Study of Nanobubble Dynamics. *Phys. Rev. Lett.* **109**, 174501 (2012).
- Zhang, X. H., Chan, D. Y. C., Wang, D. Y. & Maeda, N. Stability of Interfacial Nanobubbles. *Langmuir* **29**, 1017–1023 (2013).
- Huang, T. W. *et al.* Dynamics of hydrogen nanobubbles in KLH protein solution studied with in situ wet-TEM. *Soft Matter* **9**, 8856–8861 (2013).
- Ljunggren, S. & Eriksson, J. C. The lifetime of a colloid-sized gas bubble in water and the cause of the hydrophobic attraction. *Colloid Surface A* **130**, 151–155 (1997).
- Zhang, X. H. *et al.* Detection of novel gaseous states at the highly oriented pyrolytic graphite-water interface. *Langmuir* **23**, 1778–1783 (2007).
- Zhang, X. H., Maeda, N. & Hu, J. Thermodynamic Stability of Interfacial Gaseous States. *J. Phys. Chem. B* **112**, 13671–13675 (2008).
- Zhang, L. J., Zhang, X. H., Fan, C. H., Zhang, Y. & Hu, J. Nanoscale Multiple Gaseous Layers on a Hydrophobic Surface. *Langmuir* **25**, 8860–8864 (2009).
- Zhang, X. H. & Maeda, N. Interfacial Gaseous States on Crystalline Surfaces. *J. Phys. Chem. C* **115**, 736–743 (2011).
- Johnson, P. B. & Mazey, D. J. Helium Gas Bubble Lattices in Face-Centered-Cubic Metals. *Nature* **276**, 595–596 (1978).
- Johnson, P. B. & Mazey, D. J. Helium Gas Bubble Super-Lattice in Copper and Nickel. *Nature* **281**, 359–360 (1979).
- Evans, J. H., Vanveen, A. & Caspers, L. M. Formation of Helium Platelets in Molybdenum. *Nature* **291**, 310–312 (1981).
- Donnelly, S. E. The density and pressure of helium in bubbles in implanted metals: a critical review. *Radiat. Effects* **90**, 1–47 (1985).
- Johnson, P. B., Thomson, R. W. & Mazey, D. J. Large Bubble-Like Features Ordered on a Macrolattice in Helium-Implanted Gold. *Nature* **347**, 265–267 (1990).
- Felde, A. V. *et al.* Pressure of Neon, Argon, and Xenon Bubbles in Aluminum. *Phys. Rev. Lett.* **53**, 922–925 (1984).
- Donnelly, S. E. & Rossouw, C. J. Lattice Images of Solid Xenon Precipitates in Aluminum at Room-Temperature. *Science* **230**, 1272–1273 (1985).
- Rossouw, C. J. & Donnelly, S. E. Superheating of small solid-argon bubbles in aluminum. *Phys. Rev. Lett.* **55**, 2960–2963 (1985).
- Evans, J. H. & Mazey, D. J. Evidence for Solid Krypton Bubbles in Copper, Nickel and Gold at 293-K. *J. Phys. F Met. Phys.* **15**, L1–L6 (1985).
- Templier, C., Gaboriaud, R. J. & Gareme, H. Precipitation of Implanted Xenon in Aluminum. *Mater. Sci. Eng.* **69**, 63–66 (1985).
- Birtcher, R. C. *et al.* Behavior of crystalline Xe nanoprecipitates during coalescence. *Phys. Rev. Lett.* **83**, 1617–1620 (1999).
- Donnelly, S. E. *et al.* Ordering in a fluid inert gas confined by flat surfaces. *Science* **296**, 507–510 (2002).
- Song, M. *et al.* Structure of nanometre-sized Xe particles embedded in Al crystals. *J. Microsc.* **215**, 224–229 (2004).
- Iakoubovskii, K., Mitsuishi, K. & Furuya, K. Structure and pressure inside Xe nanoparticles embedded in Al. *Phys. Rev. B* **78**, 064105 (2008).
- Donnelly, S. E., Evans, J. H. & North Atlantic Treaty Organization. Scientific Affairs Division. *Fundamental aspects of inert gases in solids* (Plenum Press, New York, 1991).
- Chen, J., Jung, P. & Trinkaus, H. Evolution of Helium Platelets and Associated Dislocation Loops in  $\alpha$ -SiC. *Phys. Rev. Lett.* **82**, 2709–2712 (1999).
- Faraci, G., Pennisi, A. R., Terrasi, A. & Mobilio, S. Xe bubbles in Si observed by extended x-ray-absorption fine-structure spectroscopy. *Phys. Rev. B* **38**, 13468–13471 (1988).
- Hwang, I. S., Yang, C. W. & Lu, Y. H. Evidence of epitaxial growth of molecular layers of dissolved gas at a hydrophobic/water interface. *arXiv* 1203.6696 (2012).
- Lu, Y. H., Yang, C. W. & Hwang, I. S. Molecular Layer of Gaslike Domains at a Hydrophobic-Water Interface Observed by Frequency-Modulation Atomic Force Microscopy. *Langmuir* **28**, 12691–12695 (2012).
- Yang, C. W., Lu, Y. H. & Hwang, I. S. Condensation of dissolved gas molecules at a hydrophobic/water interface. *Chin. J. Phys.* **51**, 250–262 (2013).
- Lu, Y. H., Yang, C. W. & Hwang, I. S. Atomic Force Microscopy Study of Nitrogen Molecule Self-Assembly at the HOPG-Water Interface. *Appl. Surf. Sci.* **304**, 56–64 (2014).
- Weijts, J. H. & Lohse, D. Why Surface Nanobubbles Live for Hours. *Phys. Rev. Lett.* **110**, 054501 (2013).
- Israelachvili, J. N. *Intermolecular and surface forces* 3rd edn, (Academic Press, San Diego, CA, 2011).
- Hirschfelder, J. O., Curtiss, C. F., Bird, R. B. & University of Wisconsin. Theoretical Chemistry Laboratory. Molecular theory of gases and liquids. Corrected printing with notes added. edn., 1110–1112 (Wiley, New York, 1965).
- Venables, J. Introduction to surface and thin film processes Ch. 4, 108–143 (Cambridge University Press, New York, 2000).
- Vidali, G., Ihm, G., Kim, H. Y. & Cole, M. W. Potentials of Physical Adsorption. *Surf. Sci. Rep.* **12**, 135–181 (1991).
- Da Silva, J. L. F., Stampfl, C. & Scheffler, M. Adsorption of Xe atoms on metal surfaces: New insights from first-principles calculations. *Phys. Rev. Lett.* **90**, 066104 (2003).
- Granick, S., Zhu, Y. X. & Lee, H. Slippery questions about complex fluids flowing past solids. *Nat. Mater.* **2**, 221–227 (2003).
- Giessibl, F. J. Advances in atomic force microscopy. *Rev. Mod. Phys.* **75**, 949–983 (2003).
- Yang, C. W., Hwang, I. S., Chen, Y. F., Chang, C. S. & Tsai, D. P. Imaging of soft matter with tapping-mode atomic force microscopy and non-contact-mode atomic force microscopy. *Nanotechnology* **18**, 084009 (2007).
- Leung, C. *et al.* Atomic Force Microscopy with Nanoscale Cantilevers Resolves Different Structural Conformations of the DNA Double Helix. *Nano Lett.* **12**, 3846–3850 (2012).
- Ido, S. *et al.* Beyond the Helix Pitch: Direct Visualization of Native DNA in Aqueous Solution. *ACS Nano* **7**, 1817–1822 (2013).
- Adamcik, J., Berquand, A. & Mezzenga, R. Single-step direct measurement of amyloid fibrils stiffness by peak force quantitative nanomechanical atomic force microscopy. *Appl. Phys. Lett.* **98**, 193701 (2011).
- Yang, C. W., Lu, Y. H. & Hwang, I. S. Imaging surface nanobubbles at graphite-water interfaces with different atomic force microscopy modes. *J. Phys.: Condens. Matter* **25**, 184010 (2013).
- Haynes, W. M. *CRC Handbook of Chemistry and Physics* 93<sup>rd</sup> Ed. (CRC Press, Boca Raton, FL, 2012).

## Acknowledgments

We thank the National Science Council of the R.O.C. (NSC99-2112-M-001-029-MY3 and NSC102-2112-M-001-024-MY3) and Academia Sinica for supporting this study.



## Author contributions

I.-S.H. initiated and supervised the project. I.-S.H. and Y.-H.L. wrote the main manuscript text; Y.-H.L., C.-W.Y., C.-K.F., H.-C.K. and E.F. conducted experiments; Y.-H.L. prepared figures 1-3; I.-S.H. and Y.-H.L. prepared figure 4 and Table 1. All authors reviewed the manuscript.

## Additional information

Supplementary information accompanies this paper at <http://www.nature.com/scientificreports>

**Competing financial interests:** The authors declare no competing financial interests.

**How to cite this article:** Lu, Y.-H., Yang, C.-W., Fang, C.-K., Ko, H.-C. & Hwang, I.-S. Interface-Induced Ordering of Gas Molecules Confined in a Small Space. *Sci. Rep.* 4, 7189; DOI:10.1038/srep07189 (2014).



This work is licensed under a Creative Commons Attribution-NonCommercial-NoDerivs 4.0 International License. The images or other third party material in this article are included in the article's Creative Commons license, unless indicated otherwise in the credit line; if the material is not included under the Creative Commons license, users will need to obtain permission from the license holder in order to reproduce the material. To view a copy of this license, visit <http://creativecommons.org/licenses/by-nc-nd/4.0/>